Monatshefte für Chemie 134, 165–182 (2003)
DOI 10.1007/s00706-002-0537-0

Monatshefte für Chemie
Chemical Monthly
Printed in Austria

Invited Review

Spin Crossover Properties of the [Fe(*PM-BiA*)$_2$(NCS)$_2$] Complex – *Phases I* and *II*

Jean-François Létard[1,*], **Guillaume Chastanet**[1], **Olivier Nguyen**[1], **Silvia Marcén**[1], **Mathieu Marchivie**[1], **Philippe Guionneau**[1,*], **Daniel Chasseau**[1], and **Philipp Gütlich**[2]

[1] Groupe des Sciences Moléculaires, Institut de Chimie de la Matière Condensée de Bordeaux, UPR CNRS No. 9048, F-33608 Pessac, France
[2] Institut für Anorganische Chemie und Analytische Chemie, Universität Mainz, D-55099 Mainz, Germany

Received August 26, 2002; accepted August 30, 2002
Published online November 21, 2002

Summary. In the present review, we reexamine the photomagnetic properties of the [Fe(*PM-BiA*)$_2$(NCS)$_2$], *cis*-bis(thiocyanato)-bis[(*N*-2′-pyridylmethylene)-4-(aminobiphenyl)]iron(II), compound which exhibits, depending on the synthetic method, an exceptionally abrupt spin transition (*phase I*) with a very narrow hysteresis ($T_{1/2}\downarrow = 168$ K and $T_{1/2}\uparrow = 173$ K) or a gradual spin conversion (*phase II*) occurring at 190 K. In both cases, light irradiation in the tail of the ^{1}MLCT-LS absorption band, at 830 nm, results in the population of the high-spin state according to the light-induced excited spin-state trapping (LIESST) effect. The capacity of a compound to retain the light-induced HS information, estimated through the *T*(LIESST) experiment, is determined for both phases. Interestingly, the shape of the *T*(LIESST) curve is more gradual for the *phase II* than for the *phase I* and the *T*(LIESST) value is found considerably lower in the case of the *phase II*. The kinetics parameters involved in the photo-induced high-spin → low-spin relaxation process are estimated for both phases. From these data, the experimental *T*(LIESST) curves are simulated and the particular influence of the cooperativity as well as of the parameters involved in the thermally activated and tunneling regions are discussed. The Light-Induced Thermal Hysteresis (LITH), originally described for the strongly cooperative *phase I*, is also reinvestigated. The quasi-static LITH loop is determined by recording the photostationary points in the warming and cooling branches.

Keywords. Spin crossover; Iron(II); Photomagnetism; Kinetic relaxation.

* Corresponding authors. E-mail: letard@icmcb.u-bordeaux.fr

1. Introduction

Today, a promising strategy in the development of information technology is offered by the small-upward (bottom-up) approach where molecules or assemblies of molecules are used for information processing [1]. In this context, molecular bistability, that is the ability of a molecular system to occur in two different electronic states, is a particularly interesting property since logic operations can be executed. One of the most fascinating example of molecular bistability is certainly given by the spin crossover (SC) phenomenon discovered by *Cambi et al.* in 1931 on iron(III) dithiocarbamate complexes [2], and some 30 years later by *Baker* and *Bobonich* on the first iron(II) coordination compound [3]. Many examples of SC complexes, particularly of iron(II) and iron(III) became shown thereafter [4–6]. In fact, it is only during the 1980's that researchers realized that SC compounds could be used as active elements in memory devices [7] and the iron(II) transition metal ion was particularly studied [8]. In this latter metal case, at the molecular scale, the SC phenomenon corresponds to an intra-ionic transfer of two electrons occurring in the nanosecond scale between the e_g and t_{2g} orbitals. The phenomenon may be induced by a change of temperature, of pressure, or by light irradiation [8].

The first photomagnetic effect on an iron(II) SC compound was reported by *Decurtins et al.* in 1984 [9]. The authors demonstrated the possibility to convert a low-spin (LS) state into a metastable high-spin (HS) state at sufficiently low temperatures ($\leq$50 K) by using green light irradiation. This phenomenon was named the Light-Induced Excited Spin-State Trapping (LIESST effect). Later on, *Hauser* proved that red light switches the system back from the HS to the LS state (reverse-LIESST) [10]. Today, the LIESST effect has been observed in a large number of iron(II) systems [8, 11]. From all these examples, we have learned that due to the large increase in metal-ligand bond lengths during the light-induced population of the HS state at low temperatures, the role of the elastic interactions are particularly important for the interpretation of the photomagnetic data [12]. The resulting elastic interactions may be pictured as an internal pressure which is proportional to the concentration of the low-spin species. In diluted systems, the HS $\rightarrow$ LS relaxation is single exponential whereas in concentrated systems the curves follow a sigmoidal behavior due to a self-accelerating process resulting from the cooperative interactions.

Another important feature of the LIESST effect is that trapping the system in a metastable HS state requires very low temperatures. Usually, above 50 K, the metastable HS state decays within minutes and the "information" is erased. The relaxation process follows the non-adiabatic multi-phonon theory with a temperature independent HS $\rightarrow$ LS relaxation below $\sim$50 K [13] and a thermally activated process at elevated temperature which can be regarded as a tunneling from thermally populated vibrational levels of the HS state [14]. Nevertheless, in some unexplained cases, long-lived metastable HS states have been reported even at elevated temperatures [15, 16], suggesting that some unknown secondary reactions in the nearby lattice surroundings of a light-generated HS complex molecule are able to stabilize the metastable HS state. In this context, we have introduced the notion of critical LIESST temperature, T(LIESST), defined as the temperature for which the light-induced HS information is erased [17]. Our idea was to constitute a data base which collects the photomagnetic properties of a large number of iron(II) SC compounds. Today, more than thirty SC compounds have been characterized with the same T(LIESST)

procedure. It seems already that a direct relation exists between the T(LIESST) value and the thermal spin transition temperature, ($T_{1/2}$); *i.e.* $T(\text{LIESST}) = T_0 - 0.3T_{1/2}$ with T_0 estimated at $T \rightarrow 0$ [18, 19]. The influence of the coordination sphere (nature of the organic core, of the anion, of the hydration degree) and of the cooperativity on the magnitude of the T(LIESST) is currently investigated [19].

In the present paper, we review the particular case of the [Fe(*PM-BiA*)$_2$(NCS)$_2$], *cis*-bis(thiocyanato)-bis[(*N*-2′-pyridylmethylene)-4-(aminobiphenyl)] iron(II), compound. This system has been selected by reason of the presence of two phases exhibiting different magnetic and photomagnetic properties [17, 20–27]. The thermal SC regimes is either gradual (*phase II*) or exceptionally abrupt (*phase I*) with a narrow hysteresis of ca. 5 K ($T_{1/2}\downarrow = 168$ K and $T_{1/2}\uparrow = 173$ K) and, consequently, the particular role of the cooperativity on the T(LIESST) value will be investigated.

In Section 2, some highlights concerning the thermal spin crossover properties of the [Fe(*PM-BiA*)$_2$(NCS)$_2$] compound will be recalled. In Section 3, on the basis of new results the photomagnetic properties of both phases will be reexamined. The Light-Induced Thermal Hysteresis (LITH) [17], originally described for the strongly cooperative *phase I*, will also be reinvestigated. The various kinetics parameters involved in the HS $\rightarrow$ LS relaxation will be determined and the T(LIESST) curve will be simulated. In Section 4, the kinetics parameters of the strongly cooperative *phase I* will be compared to the weak cooperative *phase II*. The influence of these parameters on the T(LIESST) value will be analyzed.

2. Highlights on the [Fe(*PM-BiA*)$_2$(NCS)$_2$] Complex

2.1. Synthesis

The first description of the synthesis of the [Fe(*PM-BiA*)$_2$(NCS)$_2$] complex was reported in 1997 and the analysis of the SC properties recorded for the powder sample form gave a gradual spin transition [20]. Later on in 1998, we have reported that a change of the synthetic conditions allowed to obtain a new phase with an exceptionally abrupt spin transition [17]. The abrupt form was arbitrarily named *phase I* and the gradual spin conversion *phase II*. Today, the synthesis of the two phases has been performed several times. From all these experiments, we have learned that the main difference in the synthesis procedure concerns the speed to obtain the [Fe(*PM-BiA*)$_2$(NCS)$_2$] complex. In some intermediate case, the final powder compound corresponds to a mixture of both phases and the magnetic data revealed the summation of both behavior.

The procedure to obtain the *phase I* was as following. Under nitrogen atmosphere, 2.7 g of iron(II) sulfate heptahydrate, $Fe(SO_4)_2 \cdot 7H_2O$, (9.7 mmol) and 1.8 g of potassium thiocyanate, KNCS, (19 mmol) were dissolved in 20 cm^3 of freshly distillated methanol [17]. The presence of ascorbic acid was used to prevent the iron(II) oxidation. The colorless solution of $Fe(NCS)_2$ was separated from the white precipitate of potassium sulfate by filtration, and added dropwise to a stoichiometric amount of *PM-BiA*, *N*-2′-pyridyl-methylene-4-aminobiphenyl (5 g, 19 mmol) in 20 cm^3 of methanol. The green [Fe(*PM-BiA*)$_2$(NCS)$_2$] precipitate was then slowly formed. The *PM-BiA* ligand was synthesized from the 2-pyridinecarbaldehyde and the aminobiphenyl.

The *phase II* was obtained by a fast precipitation of the [Fe(*PM-BiA*)$_2$(NCS)$_2$] complex [20, 21]. For this, we have used an excess of *PM-BiA* ligand (1 g, 3.88 mmol) in regard to $Fe(SO_4)_2 \cdot 7H_2O$, (0.27 g, 0.97 mmol) and KNCS (0.189 g, 1.94 mmol) constituents and moreover the methanol quantity was limited to 5 cm^3.

2.2. Thermal Spin Transition Behavior

Figure 1 compares the spin transition properties recorded for the two phases of the [Fe(*PM-BiA*)$_2$(NCS)$_2$] compound [17, 20–22]. At room temperature, the $\chi_M T$ product (χ_M stands for the molar magnetic susceptibility and T the temperature) is close to 3.5 cm^3 K mol^{-1}, corresponding to what is expected for a quintet HS ground state. When the temperature is lowered, the magnetic signal of the *phase II* gradually decreases while the $\chi_M T$ product of the *phase I* drops suddenly within 2 K around 168 K. Below 150 K, the magnetic responses of both phases are close to zero, indicating the presence of solely a singlet LS ground state. In the warming mode, the $\chi_M T$ product of the *phase II* smoothly increases and the magnetic data perfectly correspond to those obtained in the cooling mode, showing that a complete gradual spin transition occurs at $T_{1/2} = 198$ K without thermal hysteresis (Fig. 1a). For *the phase I*, the magnetic data recorded during the warming mode abruptly increase, within 1 K, at 173 K. The compound exhibits a complete abrupt spin transition with a thermal hysteresis loop of 5 K ($T_{1/2}\downarrow = 168$ K and $T_{1/2}\uparrow = 173$ K, see Fig. 1b).

The thermal spin crossover properties of the *phase I* has also been investigated by *Mössbauer* spectroscopy. Figure 2 shows a representative series of *Mössbauer* spectra recorded at various temperatures. From the spectra recorded at 200 K (and above) and at 140 K (and below), it has been checked that the thermal spin transition of the *phase I* is complete. For instance, the spectrum at 200 K presents a unique doublet characteristic of iron(II) in HS state, the isomer shift δ being 0.91(1) mm/s (relative to α-iron) and a quadrupole splitting E_Q being 2.82(1) mm/s, while the spectrum at 140 K shows only the doublet characteristic of the iron(II) LS state with

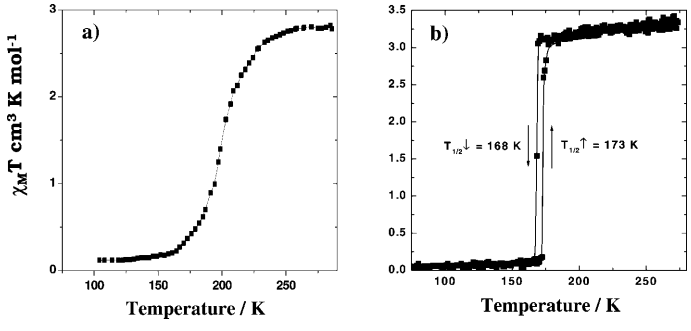

Fig. 1. $\chi_M T$ product *vs.* T (χ_M stands for the molar magnetic susceptibility and T the temperature) in the 80–300 K region of [Fe(*PM-BiA*)$_2$(NCS)$_2$] in both warming and cooling modes. (a) *phase II*; (b) *phase I*. The thermal spin transition has been followed with a Manics DSM-8 fully automatized *Faraday*-type magnetometer equipped with an DN-170 Oxford Instruments continuous-flow cryostat and a BE 15f Bruker electromagnet operating at *ca.* 0.8 Tesla and in the 80–300 K temperature range

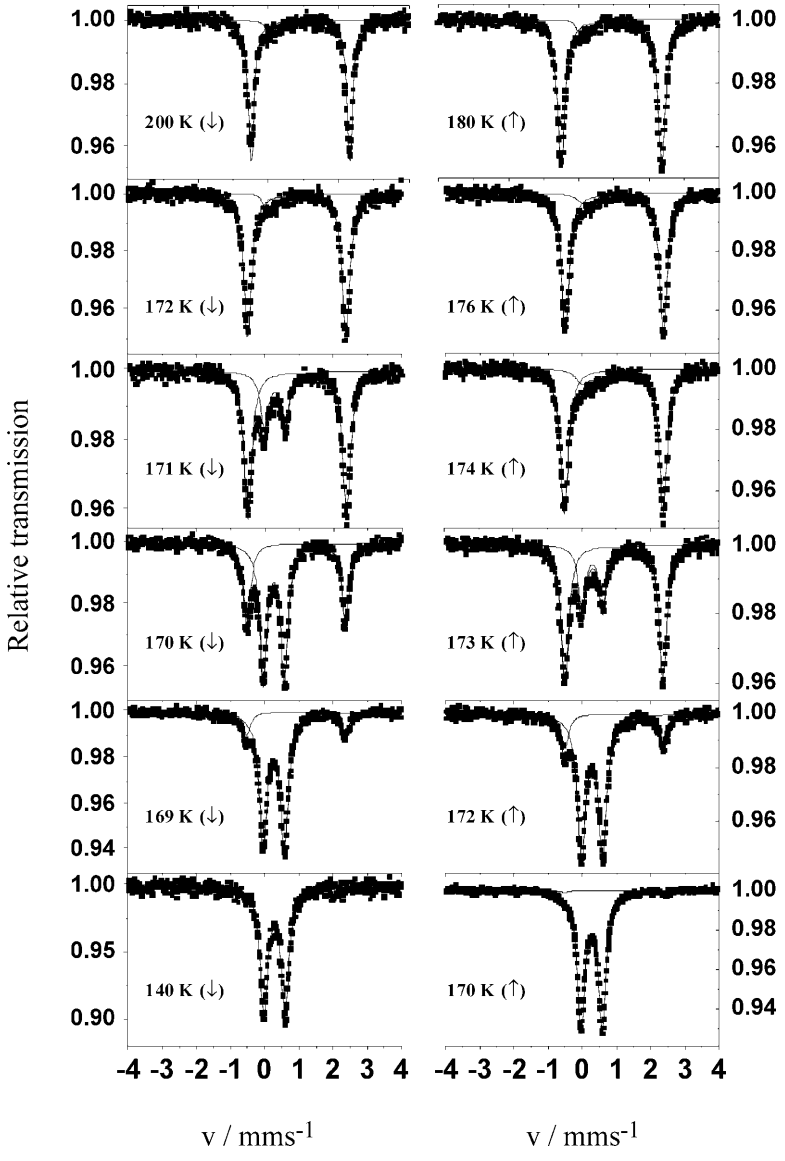

Fig. 2. *Mössbauer* spectra of *phase I* at different temperatures

$\delta = 0.28(1)\,\mathrm{mm/s}$ and $E_Q = 0.62(1)\,\mathrm{mm/s}$. The spectra recorded in the vicinity of the 168–172 K region show the coexistence of the two spin isomers with strongly temperature-dependent relative intensities. Figure 3 reports the calculated HS area fractions as function of the temperature during the cooling and warming modes. This result has confirmed the exceptional abrupt character of the thermal spin transition and the presence of a thermal hysteresis of 5 K obtained by magnetic susceptibility measurements.

In the particular case of the strongly cooperative *phase I*, pressure experiments have also been performed [22]. The aim was to study the effect of an external pressure on the hysteresis loop. Figure 4 recalls the magnetic properties obtained

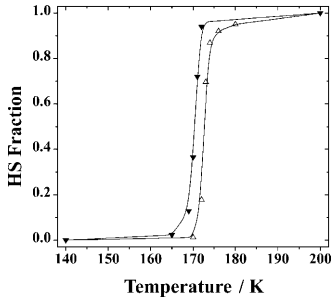

Fig. 3. Plot of the HS fraction *vs. T* of *phase I* determined by *Mössbauer* spectroscopy in the warming and the cooling modes

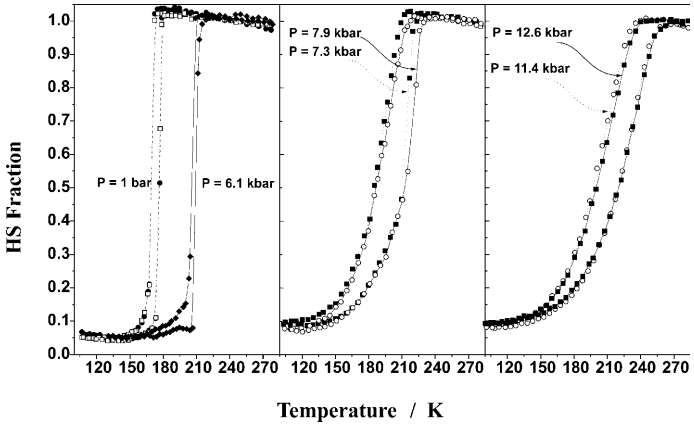

Fig. 4. HS fraction under hydrostatic pressures for the *phase I*

under hydrostatic pressure. When the pressure increases from 1 bar to 6.1 kbar, the transition temperature $T_{1/2}$ was observed to shift upwards and the width of the hysteresis was reduced. At higher pressures, 7.3 kbar and 7.9 kbar, the hysteresis width became large (25 K), and beyond 10 kbar, the spin crossover was found to become more gradual and the hysteresis width slightly diminished. The increase of the hysteresis loop in the vicinity of 7–8 kbar has been interpreted as the presence of a new phase transition [22]. Nevertheless, whatever the nature reached in the high pressure domain, these data show that the width of the thermal hysteresis remains smaller than 25 K. It was not possible to drastically affect the cooperativity of the *phase I*, linked to the supramolecular organization of the aromatic ligand, by an external pressure perturbation.

2.3. X-Ray Investigation

The [Fe(*PM-BiA*)$_2$(NCS)$_2$] compound is a member of the [Fe(*PM-L*)$_2$(NCS)$_2$] family with *PM-L* the *N*-2′-pyridylmethylene-4-aminoaryl ligand. Interestingly, this family of complexes offers a large diversity of the spin conversion features together with, in a first approach, similarities in the structural properties [23–27]. A careful comparative examination of the crystal structures determined both in the

HS and the LS states sheds light on some differences within the crystal packing. These differences have turned out to be directly connected to the diversity of the spin conversion features. For instance, the paramount role of hydrogen bonds has been pointed out.

The crystal structures of the *phase I* have been determined at 293 K, 140 K [17] and 30 K [25] and those of *phase II* at 293 K and 120 K [27]. The temperature dependence of the cell parameters has also been determined for both phases and the thermal expansion tensors discussed [23–27]. It is important to note that the single crystals of *phase I* and *phase II* are hardly differentiable by microscope observation as they show no significant differences in morphology. In order to identify the nature of a batch of samples (in powder or single crystal form), a quick X-ray powder experimental diffractogram have been compared to the ones calculated from the single crystal X-ray crystal structures of the two phases. Indeed, the *phase I* and *phase II* diffractograms appear to be notably different (Fig. 5).

At room temperature, *phase I* crystallises in the orthorhombic space group Pccn ($a = 12.949(7)$ Å, $b = 15.183(2)$ Å, $c = 17.609(5)$ Å, $V = 3462(2)$ Å^3) and *phase II* in the monoclinic space group $P2_1/c$ ($a = 17.358(5)$ Å, $b = 12.602(2)$ Å, $c = 17.570(5)$ Å, $\beta = 115.68(1)^\circ$, $V = 3464(2)$ Å^3). Interestingly, the unit cell volumes of both phases are identical and the unit cell contains four entities. In the orthorhombic phase, iron atoms lie on a two-fold axis and consequently the molecule is symmetrical, which is not the case in the monoclinic phase. The main intramolecular differences in the *phase II* concerns one of the two external phenyl groups of the complex which displays very large atomic displacement parameters. Otherwise, the geometry of the FeN_6 octahedron is very similar in both phases at room temperature. For instance, the Fe–N bond lengths as well as the associated distortion parameter Σ of the two phases are very similar. Likewise, despite the difference in space group, the crystal packing is also similar (Fig. 6). One of the differences comes from the perfect alignment of the iron atoms, for symmetrical reasons, in *phase I* while these atoms form a zigzag arrangement in *phase II*. The packing is driven by π–π interactions between neighbouring complexes as well as intermolecular hydrogen like contacts involving the NCS branches. These intermolecular interactions show some

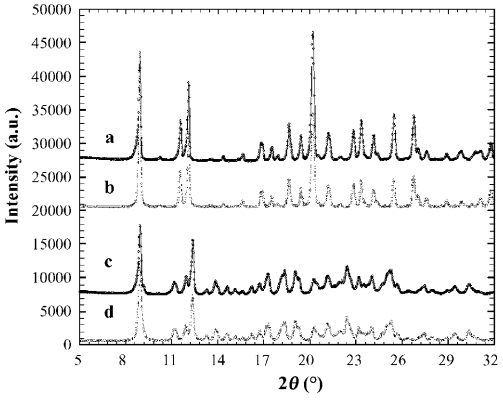

Fig. 5. Simulated and experimental powder diffractograms of [Fe(*PM-BiA*)$_2$(NCS)$_2$] in *phase I* (a, b respectively) and in *phase II* (c, d respectively)

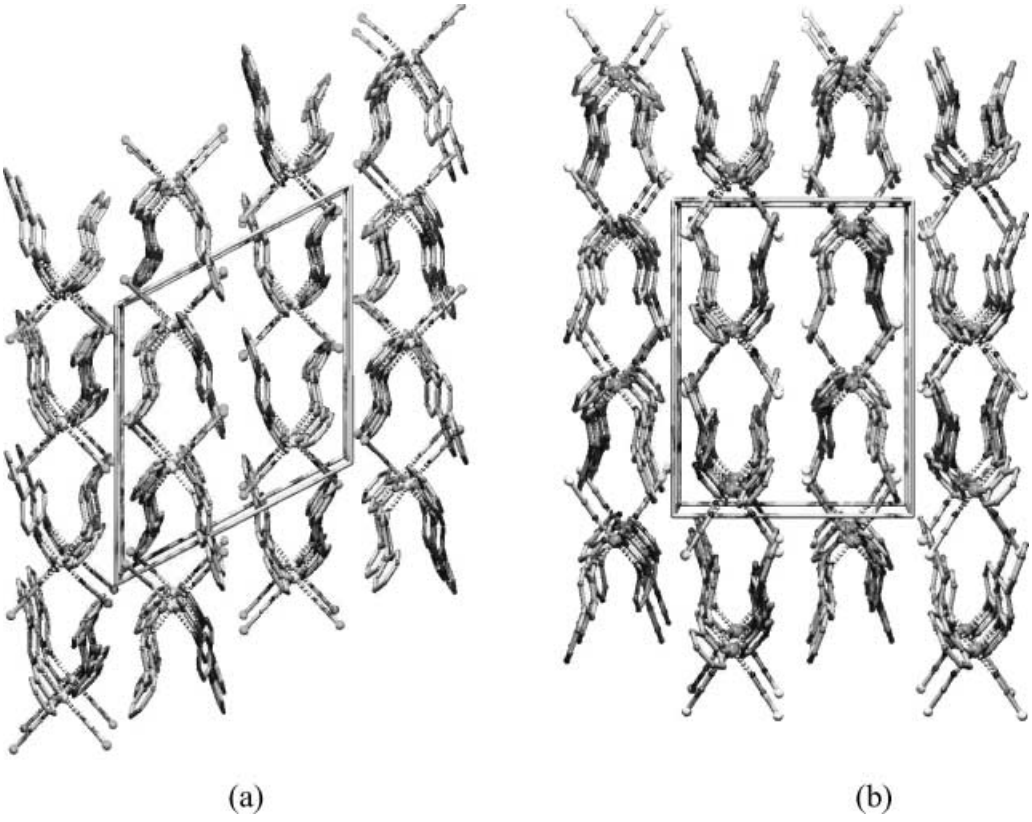

Fig. 6. Crystal packing and unit cell of [Fe(*PM-BiA*)$_2$(NCS)$_2$] in the monoclinic phase (a) and in the orthorhombic phase (b)

small differences in both structures but the main difference involves the sulphur atoms. Indeed, the intermolecular hydrogen like contacts S···HC is significantly shorter in *phase I* (S···C: 3.41(1) Å) than in *phase II* (S···C: 3.54(1) Å).

At low temperature, below the spin crossover, no essential modification occurs in the crystal structures. From 293 K to 140 K, the amplitude of contraction of the unit cell is slightly larger in *phase II* (149 Å^3) than in *phase I* (125 Å^3). On going from HS to LS, the amplitude of the geometrical modifications of the FeN_6 octahedron are comparable: the average variation of bond lengths is $\Delta r = 0.218$ Å in *I* and $\Delta r = 0.200$ Å in *II* and the Σ parameter decreases by 39° in *I* and 37° in *II*. The FeN_6 octahedron volume is reduced by 3 Å^3 at the spin crossover in both phases like for all the Fe(II) complexes investigated up to now [26]. Interestingly, the length of the intermolecular hydrogen like contacts S···HC, discussed above, becomes identical for both phases in the low spin state: S···C: 3.44(1) Å for *phase I* and 3.45(1) Å for *phase II*.

3. Light-Induced Excited Spin-State Trapping (LIESST)

3.1. UV-Visible Absorption

The absorption spectra of [Fe(*PM-BiA*)$_2$(NCS)$_2$] have been performed for both phases at room temperature under various experimental conditions, in KBr pellet,

in cellulose acetate film, as well as in solution of acetonitrile and of butyronitrile. All the spectra are similar. In acetonitrile, the electronic absorption spectrum contains mainly three absorption bands at 256 nm ($\varepsilon = 38000\,\mathrm{l\,mol^{-1}\,cm^{-1}}$), at 337 nm ($\varepsilon = 22600\,\mathrm{l\,mol^{-1}\,cm^{-1}}$) and at 585 nm ($\varepsilon = 1230\,\mathrm{l\,mol^{-1}\,cm^{-1}}$). This spectrum is typical for an iron(II) spin-crossover compound where the metal ion is conjugated with an aromatic ring [28, 29]. The electronic transitions below 350 nm can be assigned to the $\pi \rightarrow \pi^*$ transitions of the *PM-BiA* ligand and those around 590 nm to the metal-to-ligand charge-transfer bands of the LS state (^{1}MLCT-LS).

The evolution of the UV-visible spectra as function of temperature has been followed in butyronitrile solution and in cellulose acetate film. In both cases, the decrease of the temperature results in an enhancement of the ^{1}MLCT-LS band. At low temperature, the general aspect of the UV-Visible spectra recorded at room temperature is conserved and the color of the compound remains unchanged. This particular finding contrasts with what happens for tetrazole and triazole SC derivatives, where the spin transition is accompanied by a drastic color change between violet (or pink) in the LS state and white in the HS state [7]. In fact, in the [Fe(*PM-BiA*)$_2$(NCS)$_2$] compound, the intense and broad ^{1}MLCT-LS band situated in the visible range totally overlaps with the forbidden d–d transitions of the LS and HS states and any temperature dependence of the d–d transitions remains insignificant.

3.2. LIESST Experiments

In 1998, it was reported that the metastable HS state can be generated at 10 K by irradiating the *phase I* with a Kr^+ Laser ($\lambda = 647.1$–676.4 nm), through the well-known LIESST effect. One year later, a similar behavior was described for the *phase II*. In both cases, the photoinduced HS fraction at 10 K was estimated to be around 20%. Figure 7 shows the photomagnetic properties recorded on both phases by irradiating with a diode laser emitting at 830 nm. Obviously, the magnetic signal at 10 K under irradiation rapidly increases. The $\chi_M T$ product reached after saturation

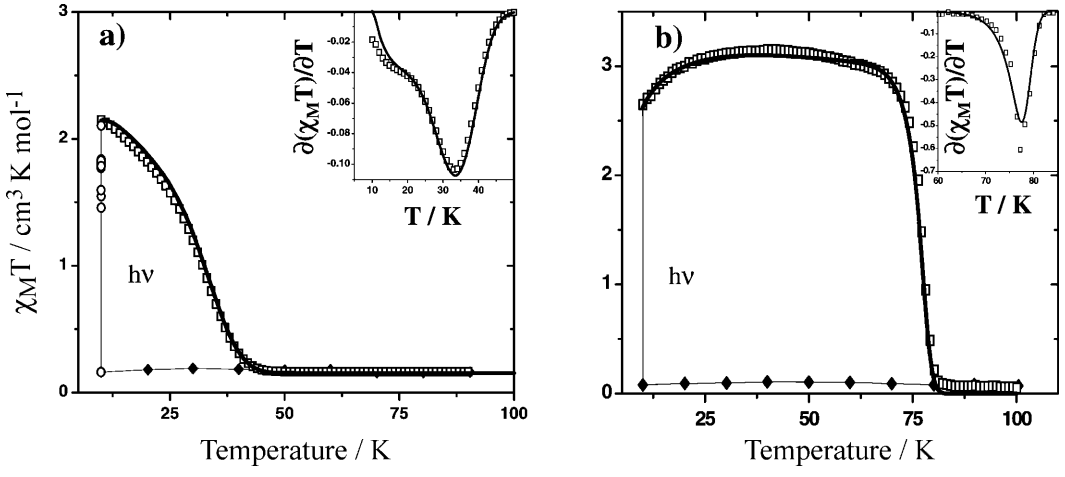

Fig. 7. Evolution of $\chi_M T$ product *vs. T* before (◆), during (o) and after (□) irradiation at 830 nm. (a) *phase II*; (b) *phase I*. The minimum of the derivative of $\chi_M T$ *vs. T* (inserts) gives the *T*(LIESST) value. The solid lines represent the simulation obtained according to Eq. (7)

was close to 2.5 $cm^3\,K\,mol^{-1}$ for the *phase I* and close to 2.1 $cm^3\,K\,mol^{-1}$ for the *phase II*. Figure 7 also reports on the *T*(LIESST) experiments. At the saturation of the magnetic signal reached under light irradiation (830 nm) at 10 K, the light was turned off and the temperature was slowly increased at a rate of 0.3 $K\,min^{-1}$. Interestingly, these *T*(LIESST) curves are strongly different. The magnetic response of the *phase II* continuously decreases with increasing temperature and the *T*(LIESST) value is 34 K. On the contrary, the $\chi_M T$ product of the *phase I* is almost independent of temperature up to *ca.* 70 K and the *T*(LIESST) value is estimated to be 78 K. The magnetic response of the *phase I* only decreases in the vicinity of 75–79 K.

From these photomagnetic data it follows: i) The increase of the magnetic signal recorded at 10 K under irradiation at 830 nm suggests that direct LIESST process occurs for both phases. This differs from the reverse-LIESST effect previously observed in these experimental conditions for tetrazole derivatives. In fact, this behavior can be understood by the presence of an intense ^{1}MLCT-LS electronic transition which totally masks the d–d transition of the HS state expected around 800–850 nm. Consequently, irradiation at 830 nm, in the ^{1}MLCT-LS absorption band, induced the population of the metastable HS state through the direct LIESST process. ii) The second remark refers to the comparison of the $\chi_M T$ product determined at the maximum of the *T*(LIESST) curves and the value recorded at room temperature. For the *phase I*, the light irradiation at 830 nm induces a nearly quantitative LS $\rightarrow$ HS photoconversion while light irradiation at 647.1–676.4 nm or at 532 nm only generates 20% of photoinduced HS fraction. This points out the particular role of the ^{1}MLCT-LS absorption band. At 830 nm the irradiation occurs on the borderline of the ^{1}MLCT-LS absorption band while at 647.1–676.4 nm or at 532 nm it is much around the maximum. Consequently, the bulk attenuation of the light intensity is lower at 830 nm than in the visible range where the opacity of the sample linked to the strong ^{1}MLCT-LS absorption prevents the light penetration. iii) The last comments concern the *T*(LIESST) experiment. From Fig. 7, it is clear that the shape of the *T*(LIESST) curves is more gradual for the *phase II* than for the *phase I*. The *T*(LIESST) experiment seems to be the mirror image of the thermal spin transition (Fig. 1). A similar comment has been recently given in the case of the $[Fe(bpp)_2]X_2 \cdot nH_2O$ series (*bpp* = 2,6-bis(pyrazol-3-yl) pyridine) [19] exhibiting gradual and abrupt thermal spin transitions. In parallel, it is also interesting to note that the *T*(LIESST) value of the *phase II* is lower than that of the *phase I*. Basically it is expected that the *T*(LIESST) value decreases with increasing $T_{1/2}$, in agreement with the inverse-energy-gap law [14] and with the recently observed relation $T(\text{LIESST}) = T_0 - 0.3T_{1/2}$ [18, 19]. However, the $T_{1/2}$ difference between both phases is only 28 K and certainly can not alone explain such drastic changes. Figure 8 shows a comparison of the relaxation kinetics recorded for both phases in the same time window.

3.3. HS → LS Relaxation

An analysis of the relaxation curves recorded for the *phase II* (Fig. 8a) shows that the kinetics can be satisfactorily fitted by using a single exponential. This behavior is, in fact, typical of a system exhibiting a weak cooperativity, as reflected by the gradual spin transition of the *phase II*. Figure 9a shows the plot of the

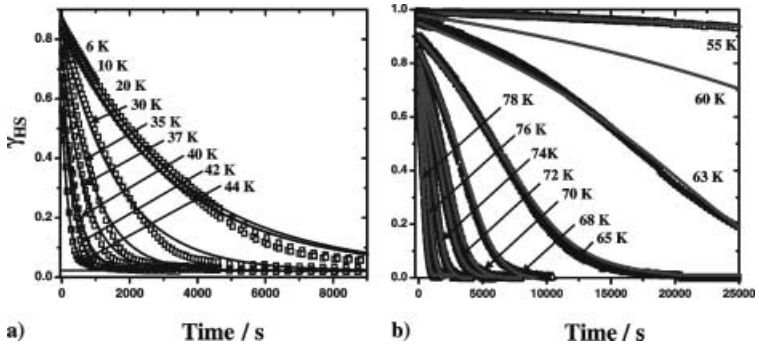

Fig. 8. Relaxation kinetics of the HS fraction *vs.* time at different temperatures. (a) *phase II*; (b) *phase I*. The solid lines represent the simulation obtained according to Eqs. (1) and (3)

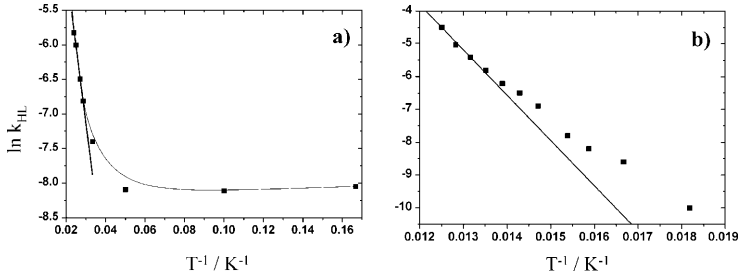

Fig. 9. *Arrhenius* plot of $\ln k_{\mathrm{HL}}(T)$ *vs.* $1/T$ for *phase II* (a) and for the *phase I* (b)

logarithm of the rate constant as function of the inverse temperature. Below 20 K, the process is found nearly temperature independent in agreement with a quantum mechanical tunneling [13] and above 20 K, the relaxation curves follow an *Arrhenius* behavior which can be regarded as a tunneling from thermally populated vibrational levels of the HS state [14]. The deduced rate constant associated to the temperature independent domain, $k_{\mathrm{HL}}(T \to 0)$, is estimated at $3 \cdot 10^{-4}\,\mathrm{s}^{-1}$. The preexponential factor in the thermally activated region, $k_\infty = 0.6\,\mathrm{s}^{-1}$, and the activation energy, $E_\mathrm{a} = 150\,\mathrm{cm}^{-1}$, are deduced from Eq. (1),

$$k_{\mathrm{HL}}(T) = k_\infty \exp(E_\mathrm{a}/k_\mathrm{B}T) \tag{1}$$

Figure 8b shows the kinetics of the *phase I*. Below 55 K, the relaxation rates are so slow that a time dependence can not be correctly estimated. For instance, at 50 K the change in HS fraction is less than 6% within 10 hours. The HS $\rightarrow$ LS relaxation kinetics becomes measurable in the time window of our SQUID setup in the 63–78 K temperature range. The most striking feature of these relaxation curves is the strong deviation from single exponential. This result perfectly agrees with the strong cooperativity of the *phase I*. In fact, it has been pointed out that elastic interactions in cooperative spin-crossover compounds act as an ''internal'' pressure in reason of the large difference in metal-ligand bond lengths between HS and LS states [8, 12, 30]. The height of the energy barrier is an increase (or a decrease) function of γ_{HS} (or γ_{LS}). In this self-acceleration process, the relaxation rate $k^*_{\mathrm{HL}}(T, \gamma_{\mathrm{HS}})$ depends exponentially on both γ_{HS} and T (Eqs. (2) and (3)), and $\alpha(T)$ is

the acceleration factor at a given temperature,

$$\frac{d\gamma_{HS}}{dt} = -k^*_{HL}\,\gamma_{HS} \tag{2}$$

$$k^*_{HL}(T, \gamma_{HS}) = k_{HL}(T)\exp[\alpha(T)(1-\gamma_{HS})] \tag{3}$$

A least-squares fit of the experimental data with $k_{HL}(T)$ and $\alpha(T)$ as free parameters is quite satisfactory. Figure 9b reports the plot of the logarithm of the rate constant, $\ln[k_{HL}(T)]$, as function of the inverse temperature. Clearly, it is difficult to deduce the kinetic parameters (activation energy and preexponential factor) involved in the thermally activated region. The true values would be only obtained at higher temperatures, in the limit regime of the thermal activation [12, 13]. The straight line of $\ln[k_{HL}(T)]$ *vs.* $1/T$ plot found in the 70–78 K region only gives access to the deduced apparent activation energy, $E_a = 1100\,cm^{-1}$, and the apparent preexponential factor, $k_\infty = 2\cdot 10^6\,s^{-1}$. Obviously, these parameters, which are certainly underestimated, are already considerably higher than those obtained for the *phase II*.

Concerning the determination of the acceleration factor $\alpha(T)$, *Hauser* has pointed out that this parameter depends on E^*_a/k_BT in the thermally activated region and reaches a limiting value, $\alpha(T\to 0)$ in the tunneling region [12]. E^*_a represents the additional activation energy linked to the cooperativity of the system. From our data, it is difficult to exactly deduce E^*_a and $\alpha(T\to 0)$. The various kinetics recorded on the 70–78 K region suggest that the magnitude of E^*_a should be in the range of $120\,cm^{-1}$. Therefore, by considering that the tunneling region acts until 40 K, the deduced limiting value $\alpha(T\to 0)$ is around 4.3. Note that the cooperativity parameter deduced from the photomagnetic data is lower than the magnitude obtained using the mean-field model proposed by *Slichter* and *Drickamer* [31] during the thermal spin transition ($\Gamma = 280\,cm^{-1}$ [32]).

An attempt to estimate the $k_{HL}(T\to 0)$ parameter for the *phase I* may lead to erroneous results in view of the long lifetimes recorded at low temperature in the tunneling region. Nevertheless, if we consider in first approximation that the k_{HL} value extrapolated from the data recorded at 63 K, where a full relaxation occurs within 11 hours, represents the upper limit of the $k_{HL}(T\to 0)$ rate constant, the deduced value is $2\cdot 10^{-5}\,s^{-1}$. Interestingly, this rate constant, which may be an overestimation of the $k_{HL}(T\to 0)$ value, is already lower than the rate constant recorded for the *phase II* ($3\cdot 10^{-4}\,s^{-1}$). This value is also lower than the previously reported values for $[Zn_{1-x}Fe_x(pic)_3]Cl_2\cdot MeOH$, $k_{HL}(T\to 0) = 9\cdot 10^{-3}\,s^{-1}$ with $T_{1/2} = 140$ K, and $[Zn_{1-x}Fe_x(mepy)_3(tren)](PF_6)_2$, $k_{HL}(T\to 0) = 1.4\cdot 10^{-1}\,s^{-1}$ with $T_{1/2} = 210$ K [33].

3.4. T(LIESST) Simulation

One way to test the validity of the various kinetic parameters, $k_{HL}(T\to 0)$, k_∞, E_a and $\alpha(T)$, is to reproduce the T(LIESST) curve. In fact, this measurement is, at least within the investigated temperature domain, a global analysis which intrinsically reflects the effects of time, temperature and cooperativity. In a measurement of a T(LIESST) curve, the sample was first irradiated at 10 K, then without further

irradiation the temperature was slowly warmed at the rate of approximately $0.3\,\mathrm{K\,min^{-1}}$. Rigorously, the temperature during a *T*(LIESST) measurement, in a SQUID cavity, is changed in 1 K steps. At each temperature T_i, the time for the signal acquisition is 60 s and the time to reach the next temperature is 120 s. In reality, it is difficult to reproduce the relaxation connected to the stabilization of the temperature. In a first approximation, we have decided to neglect this subtle effect and the relaxation is calculated at each temperature T_i during the global time of 180 s. The γ_{HS} fraction obtained after 180 s of relaxation at T_i is used as started value for the next temperature, T_{i+1}; *i.e.* $(\gamma_{HS})_{t=180}^{T=T_i} = (\gamma_{HS})_{t=0}^{T=T_{i+1}}$.

Another important point in the simulation of the *T*(LIESST) curve is that such an experiment combines the relaxation of both the tunneling and the thermally activated regions. Rigorously, this imposes to use the theory of the non-adiabatic multi-phonon process in the strong vibronic coupling limit [13]. In a first approximation, we have assumed that the evolution of the HS fraction is just a summation of the two effects. In absence of any significant cooperative effects, as for the *phase II*, the time dependence of the HS fraction at the temperature T_i is given by Eq. (4). For a cooperative compound exhibiting sigmoidal relaxation curves, as encountered for the *phase I*, Eq. (5) can be used.

$$\left(\frac{d\gamma_{HS}}{dt}\right)_{T_i} = -\gamma_{HS}\{k_{HL}(T \to 0) + k_\infty \exp(-E_a/k_B T_i)\} \tag{4}$$

$$\left(\frac{d\gamma_{HS}}{dt}\right)_{T_i} = -\gamma_{HS}\{k_{HL}(T \to 0) + k_\infty \exp(-E_a/k_B T_i)\} \exp[\alpha(T_i)(1-\gamma_{HS})] \tag{5}$$

The *T*(LIESST) curve is finally calculated by taking into account the anisotropy of the HS iron(II) ion in an octahedral surrounding. This phenomenon called zero-field splitting is associated to the spin-orbit coupling between the ground state and the excited state in a zero applied magnetic field. For an iron(II) ion in HS configuration, the S = 2 ground state is split into three levels. The magnetic contribution of each state is determined by their energy separation, *D*, and their thermal population [34]. For a powder sample, the $(\chi_M T)_{ZFS}$ product associated to the zero-field splitting and the $\chi_M T$ of the *T*(LIESST) curve are, respectively, given by Eqs. (6) and (7),

$$(\chi_M T_i)_{ZFS} = \frac{\chi_M T_{i_{//}} + 2\chi_M T_{i_\perp}}{3} \tag{6}$$

$$\text{with } \chi_M T_{i_{//}} = \frac{3}{4} g^2 \frac{e^{-D/k_B T_i} + 4e^{-4D/k_B T_i}}{1 + 2e^{-D/k_B T_i} + 2e^{-4D/k_B T_i}}$$

$$\text{and } \chi_M T_{i_\perp} = \frac{1}{4} g^2 \frac{k_B T_i}{D} \frac{9 - 7e^{-D/k_B T_i} - 2e^{-4D/k_B T_i}}{1 + 2e^{-D/k_B T_i} + 2e^{-4D/k_B T_i}}$$

$$\chi_M T_i = (\chi_M T_i)_{ZFS} \gamma_{HS}(t, T_i) \tag{7}$$

Figure 7 shows the calculated *T*(LIESST) curves of the two phases. The rate constant of the tunneling region, $k_{HL}(T \to 0)$, the preexponential factor, k_∞, the activation energy of the thermally activated region, E_a, and the acceleration factor

$\alpha(T_i)$ used are those obtained from the experimental kinetics (see Section 3.3). The agreement with the experimental data is very good. The shape and the capacity of the compound to retain the light-induced HS information, estimated through the determination of the T(LIESST), are well described. Indirectly, this demonstrates the validity of our fitting procedure as well as our estimation of the various kinetics parameters, at least, in this temperature range. The relative importance of all these kinetics parameters on the T(LIESST) will be analyzed in Section 4. The last part of this Section 3 deals with the presentation of the light-induced thermal hysteresis.

3.5. Light-Induced Thermal Hysteresis

In 1998, it was reported that under permanent irradiation the *phase I* of the $[Fe(PM\text{-}BiA)_2(NCS)_2]$ complex displays a new kind of thermal hysteresis in the vicinity of the T(LIESST) temperature [17]. This phenomenon was named the Light-Induced Thermal Hysteresis (LITH) [17]. Later on *Varret et al.* report a similar effect on the $[Fe_xCo_{1-x}(btr)_2(NCS)_2] \cdot H_2O$ system and a non-linear macroscopic master equation was proposed based on the competition between the constant photo-excitation and the self-accelerated thermal relaxation process [35].

The LITH phenomenon on the *phase I* of the $[Fe(PM\text{-}BiA)_2(NCS)_2]$ was originally observed with a Kr^+ Laser ($\lambda = 647.1$–676.4 nm) and only 20% of the light-induced HS state was populated [17]. Figure 10 displays the LITH loop obtained by irradiating the sample with a photodiode emitting at 830 nm. The sample was irradiated at 10 K until saturation of the magnetic signal, then under permanent irradiation the temperature was slowly warmed up to 100 K at the rate of 0.3 K min^{-1} and cooled back to 10 K at the rate of 0.2 K min^{-1}. In regard to the magnetic signal recorded at elevated temperatures, this experiment represents for

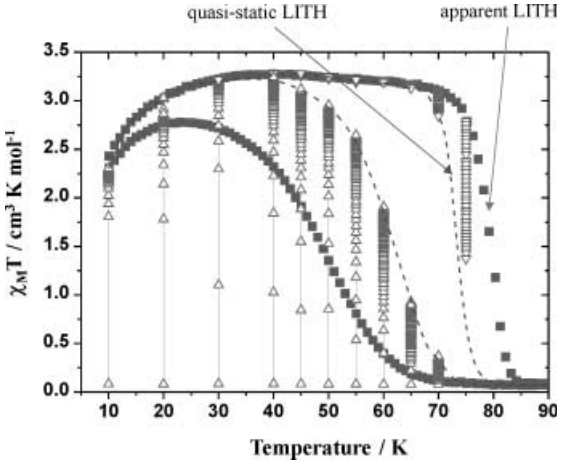

Fig. 10. Evolution of the $\chi_M T$ product *vs.* T of *phase I* under permanent irradiation at 830 nm (■) for a warming speed of 0.3 K min^{-1} and a cooling speed of 0.2 K min^{-1}. This gives the apparent LITH. (Δ) irradiation at 820 nm of the LS state for different temperatures. (∇) Irradiation at 820 nm of the HS state for different temperatures. Each irradiation leads to a photostationary point which describes the quasi-static LITH (---)

the *phase I* the first LITH loop with quantitative photoconversion. Obviously, the steepness of the warming branch is higher than of the cooling branch. We call this thermal hysteresis the *apparent* LITH loop. The *real* LITH loop will be obtained by recording the hysteresis loop with an infinite time, that is, when the steady state between the population and the relaxation is achieved. Otherwise, we are dealing with a dynamic hysteresis.

In order to approach the final form of the *real* LITH loop, we have determined some photostationary points on both the warming and the cooling branches. The procedure used was the following:

- On the cooling branch, the sample in the dark was slowly cooled down to the given temperature, T_{h_ν}. The sample was then irradiated and the $\chi_M T$ product was recorded. The experiment was stopped when the photostationary limit, equilibrium between population and depopulation, was reached. The temperature was finally warmed to 100 K and maintained at this temperature for 5 minutes to assure that any photoinduced HS fraction was erased. The T_{h_ν} was alternatively fixed at 70, 65, 60, 55, 50, 45, 40, 30, and 20 K.
- On the warming mode, the system was irradiated at 10 K until saturation, then warmed to T_{h_ν} where a new photostationary point was recorded. The T_{h_ν} was alternatively fixed at 10, 20, 30, 40, 45, 50, 55, 60, 65, and 70 K. Between each T_{h_ν}, the temperature was maintained 5 minutes at 100 K in order to erase any photoinduced HS fraction, then the sample was irradiated at 10 K until reaching the photostationary limit.

Figure 10 collects the different photostationary points and the proposed profile of the *real* LITH curve. As expected, this loop is much more narrow than the *apparent* one, *i.e.* ~10 K broad as compared to the previous 35 K. It is interesting to note that the asymmetry character of the LITH loop remains. The cooling branch is much more gradual than the warming branch. Further work is currently in progress to understand this particular behavior. The influence of various parameters, such as light intensity, as absorption of the LS/HS states, have been recently analyzed [36, 37]. It appears to be clear that the cooperativity is at the origin of the LITH phenomenon. This point is particularly well illustrated by the absence of the LITH effect in the *phase II* of the $[Fe(PM\text{-}BiA)_2(NCS)_2]$ compound. The photomagnetic signals recorded during the warming and the cooling modes are very similar.

4. Comparative Analysis of the Kinetic Parameters Involved in the *Phases I* and *II*

4.1. Cooperative Effects

Figure 11a reports the calculated *T*(LIESST) curves by using the kinetic parameters of the *phase I* as function of the additional activation energy associated to the cooperativity, E_a^*. Clearly, the shape of the *T*(LIESST) curve becomes more gradual as the cooperativity decreases. This behavior agrees with the experimental data recorded for the *phases I* and *II*. The *T*(LIESST) curve was found to be gradual for the weakly cooperative *phase II* and abrupt in the case of *phase I*.

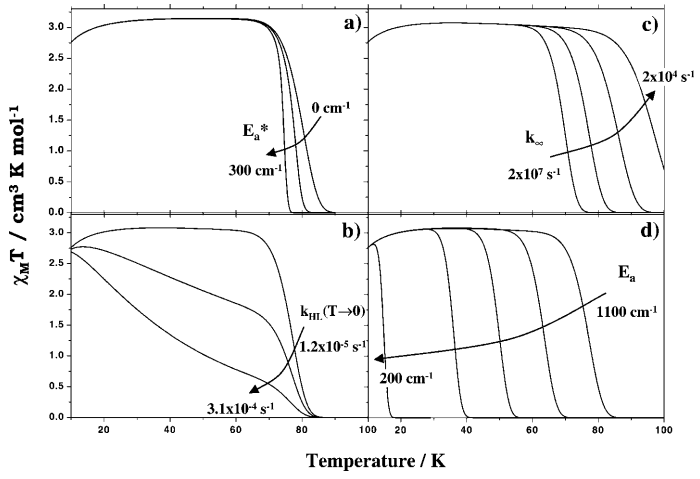

Fig. 11. Influence of the kinetics parameters on the T(LIESST) curve. (a) Variation of E_a^*; 0, 120, and 300 cm^{-1}. (b) Variation of $k_{HL}(T \to 0)$; $1.2 \cdot 10^{-5}$, $1.2 \cdot 10^{-4}$, and $3.1 \cdot 10^{-4}\,s^{-1}$. (c) Variation of k_∞; $2 \cdot 10^7$, $2 \cdot 10^6$, $2 \cdot 10^5$, and $2 \cdot 10^4\,s^{-1}$. (d) Variation of E_a; 1100, 900, 700, 500, and 200 cm^{-1}

From Figure 11a, it can also be noticed that the calculated T(LIESST) value is predicted to slightly increase when the cooperativity is reduced. This effect is linked to the increase of the height of the activation energy for a given HS fraction in Eq. (5) when E_a^* is reduced. Obviously, experimental data are inverse. The T(LIESST) value was clearly higher for the cooperative *phase I* than for the weakly cooperative *phase II*, suggesting that the main difference between the T(LIESST) values of *both phases* is not linked to a cooperativity effect. This finding is in line with the experimental results obtained from the comparison of a series of $[Fe(bpp)_2]X_2 \cdot nH_2O$ compounds, where independently to the cooperativity, the photomagnetic properties are found to follow the $T(\text{LIESST}) = T_0 - 0.3T_{1/2}$ law with $T_0 = 150$ [19].

4.2. Tunneling and Thermally Activated Regions

It is now well established that the HS $\rightarrow$ LS relaxation in general is determined by a nearly temperature-independent tunneling rate at low temperatures and an activated behavior at elevated temperatures. On the basis of a comparison between the photomagnetic properties of diluted SC compounds, *Hauser et al.* have shown that the magnitude of the low temperature tunneling rates as well as the activated region can be understood in terms of nonadiabatic multiphonon relaxation [33]. Figure 11b shows the influence of $k_{HL}(T \to 0)$ on the T(LIESST) curve by using the kinetics parameters of the *phase I* with a cooperative factor fixed at zero. Interestingly, from the values of the *phase I* ($k_{HL}(T \to 0) = 1.2\,10^{-5}\,s^{-1}$) and of the *phase II* ($3.1\,10^{-4}\,s^{-1}$), the shape of the T(LIESST) curve becomes more gradual as experimentally observed. Nevertheless, the T(LIESST) value, defined by the minimum in the derivative of the $\chi_M T$ *vs.* T plot, remains around 78 K. In the temperature-independent region, the decrease of the T(LIESST) curve is, in fact, relative to the $k_{HL}(T \to 0)$ constant and the derivative of the $\chi_M T$ *vs.* T plot gives a straight line. The minimum in the derivative of the $\chi_M T$ *vs.* T plot occurs only in the vicinity of the thermally activated region.

Figures 11c and 11d report the influence of the parameters of the thermally activated region on the *T*(LIESST) curve. A decrease of the preexponential factor, k_∞, increases the stabilization of the photoinduced HS fraction and rises the *T*(LIESST) value. This tendency is opposite to the experimental data and suggests that the change of the preexponential factor between the *phase I* ($2\,10^6\,s^{-1}$) and the *phase II* ($0.6\,s^{-1}$) can not explain the decrease of the *T*(LIESST) value. The role of the activation energy seems to be, in contrary, more important. A change between $1100\,cm^{-1}$ to $200\,cm^{-1}$ dramatically reduces the *T*(LIESST) value. At $200\,cm^{-1}$, the *T*(LIESST) value is in the expected region experimentally recorded for the *phase II*.

These results suggest that the main differences between the photomagnetic properties of the two phases are linked to the thermally activation energy. From a structural point of view, it is difficult to attribute the increase of the activation energy to a given modification of the FeN_6 core. Between both phases, the distortion of the octahedron is very similar and the crystal packing is also very close. The main difference seems to be the average of the bond lengths between the HS and the LS states which are higher for the *phase I* ($\Delta r = 0.218$ Å) than for the *phase II* (0.200 Å). Such a change is, in fact, consistent with the decrease of the activation energy on going from *phase I* ($1100\,cm^{-1}$) to *phase II* ($150\,cm^{-1}$) as well as to the observed increase of the tunneling rate constant, *i.e.* $k_{HL}(T \rightarrow 0) = 2 \cdot 10^{-5}\,s^{-1}$ for *I* instead of $3 \cdot 10^{-4}\,s^{-1}$ for *II*.

5. Conclusions

The study of the [Fe(*PM-BiA*)$_2$(NCS)$_2$] compound has shown the importance of the intense ^{1}MLCT-LS electronic transition in the photomagnetic experiments. The strong opacity of the [Fe(*PM-BiA*)$_2$(NCS)$_2$] compound in the visible range imposes to perform the photomagnetic experiments at the tail of the ^{1}MLCT-LS absorption band. Otherwise incomplete photoconversion may occur due to a bulk attenuation of light intensity. At 10 K, it was shown that light irradiation with a diode laser emitting at 830 nm induced an almost quantitative conversion to the HS state. A complete LITH loop has been described for the *phase I* of the [Fe(*PM-BiA*)$_2$(NCS)$_2$] compound. The various kinetic parameters involved in the HS $\rightarrow$ LS relaxation have been determined and used to simulate the *T*(LIESST) experiments. The influence of the cooperativity, of the tunneling and of the thermally activated kinetics parameters on the capacity of a compound to retain the metastable HS information, *i.e.* *T*(LIESST) value, have been discussed.

Acknowledgements

We are grateful for financial assistance from the European Commission for granting the TMR-Network "Thermal and Optical Switching of Spin States (TOSS)", Contract No. ERB-FMRX-CT98-0199 and from the ESF "Network Molecular Magnets" program.

References

[1] Balzani V, Credi A, Raymo FM, Stoddart JF (2000) Angew Chem Int Ed **39**: 3348
[2] Cambi L, Szegö L, Cassano A (1931) Accd Naz Lincei **13**: 809
[3] Baker WA, Bobonich HM (1964) Inorg Chem **3**: 1184

[4] König E (1968) Coord Chem Rev **3**: 471
[5] Goodwin HA (1976) Coord Chem Rev **18**: 293
[6] Gütlich P (1981) Struct Bonding (Berlin) **44**: 83
[7] Kahn O, Kröber J, Jay C (1992) Adv Mater **4**: 718
[8] Gütlich P, Hauser A, Spiering H (1994) Angew Chem Int Ed Engl **33**: 2024
[9] Decurtins S, Gütlich P, Köhler CP, Spiering H, Hauser A (1984) Chem Phys Lett **105**: 1
[10] Hauser A (1986) Chem Phys Lett **124**: 543
[11] Gütlich P, Garcia Y, Woike T (2001) Coord Chem Rev **219**: 839
[12] Hauser A, Jeftic J, Romstedt H, Hinek R, Spiering H (1999) Coord Chem Rev **190–192**: 471
[13] Bukhs E, Navon G, Bixon M, Jortner J (1980) J Am Chem Soc **102**: 2918
[14] Hauser A (1991) Coord Chem Rev **111**: 275
[15] Buchen Th, Gütlich P, Goodwin HA (1994) Inorg Chem **33**: 4573
[16] Hayami S, Gu ZZ, Einaga Y, Kobayasi Y, Ishikawa Y, Yamada Y, Fujishima A, Sato O (2001) Inorg Chem **40**: 3240
[17] Létard J-F, Guionneau P, Rabardel L, Howard JAK, Goeta AE, Chasseau D, Kahn O (1998) Inorg Chem **37**: 4432
[18] Létard J-F, Capes O, Chastanet G, Moliner N, Létard S, Real JA, Kahn O (1999) Chem Phys Lett **313**: 115
[19] Marcen S, Lecren L, Capes L, Goodwin HA, Létard J-F (2002) Chem Phys Lett **358**: 87
[20] Létard J-F, Montant S, Guionneau P, Martin P, Le Calvez A, Freysz E, Chasseau D, Lapouyade R, Kahn O (1997) Chem Commun 745
[21] Létard J-F, Daubric H, Cantin C, Kliava J, Bouhedja YA, Nguyen O, Kahn O (1999) Mol Cryst and Liq Cryst **335**: 495
[22] Ksenofontov V, Levchenko G, Spiering H, Gütlich P, Létard J-F, Bouhedja Y, Kahn O (1998) Chem Phys Lett **294**: 545
[23] Daubric H, Kliava J, Guionneau P, Chasseau D, Létard J-F, Kahn O (2000) J Phys Condens Mater **12**: 5481
[24] Guionneau P, Létard J-F, Yufit DS, Chasseau D, Bravic G, Goeta AE, Howard JAK, Kahn O (1999) J Mater Chem **9**: 985
[25] Guionneau P, Brigouleix C, Barrans Y, Goeta AE, Létard J-F, Howard JAK, Gaultier J, Chasseau D (2001) CR Acad Sci Paris, Chemistry **4**: 161
[26] Guionneau P, Marchivie M, Bravic G, Létard JF, Chasseau D (2002) J Mater Chem **12**: 2546
[27] Marchivie M, Guionneau P, Létard JF, Chasseau D, submitted to Acta Cryst B
[28] Ferguson J, Herren F (1982) Chem Phys Lett **89**: 371
[29] Hauser A, Adler J, Gütlich P (1988) Chem Phys Lett **152**: 468
[30] Gütlich P, Spiering H, Hauser A (1999) Inorganic Electronic Structure and Spectroscopy, In: Solomon EI, Lever ABP (eds) Vol II, Wiley, New York, p 575
[31] Slichter CP, Drickamer HG (1972) J Chem Phys **56**: 2142
[32] Capes L, Létard J-F, Kahn O (2000) Chem Eur **6**: 2246
[33] Hauser A, Vef A, Adler P (1991) J Chem Phys **95**: 8710
[34] Kahn O (1993) Molecular Magnetism, VCH: New York
[35] Desaix A, Roubeau O, Jeftic J, Haasnoot JG, Boukheddaden K, Codjovi E, Linarès J, Noguès N, Varret F (1998) Eur Phys J B **6**: 183
[36] Enachescu C, Constant-Machado H, Codjovi E, Linares J, Boukheddaden K, Varret F (2001) J Phys Chem Solids **62**: 1409
[37] Jeftic J, Matsarski M, Hauser A, Goujon A, Codjovi E, Linarès J, Varret F (2001) Polyhedron **20**: 1599